infrastructures

MDPI

Article

Optimization of Bolted Steel T-Stub Connection Based on Nonlinear Finite Element Analysis Using Genetic Algorithm

Péter Grubits [1], Tamás Balogh [2,3] and Majid Movahedi Rad [1,*]

[1] Department of Structural and Geotechnical Engineering, Széchenyi István University, 9026 Gyor, Hungary; grubits.peter@sze.hu
[2] Inter-CAD Ltd., 1072 Budapest, Hungary; balogh.tamas@ybl.uni-obuda.hu
[3] Department of Geotechnical and Structural Engineering, Óbuda University, 1034 Budapest, Hungary
* Correspondence: majidmr@sze.hu

Abstract: The equivalent T-stub method is frequently employed in infrastructure projects, including bridge engineering, to simplify bolted connection analysis. However, steel connections remain inherently complex due to nonlinear behavior, cost considerations, and code compliance, framing the design process as a discrete structural optimization problem. This research addresses these challenges by presenting a comprehensive calculation framework that combines the finite element method (FEM) and genetic algorithm (GA) to accurately evaluate the structural performance of bolted T-stub configurations. The proposed approach accounts for nonlinear behavior, thereby reflecting realistic structural responses. To enhance the simulation efficiency and reduce the computational time without significantly compromising accuracy, the study introduces a simplified modeling methodology. The effectiveness of the approach is demonstrated through the development and experimental validation of a selected T-stub connection. Furthermore, a parameter sensitivity analysis is conducted to showcase the range of possible outcomes, emphasizing the potential for optimization. Finally, the proposed connections were optimized using GA, highlighting the benefits of structural optimization in achieving efficient and precise designs for steel connections.

Keywords: T-stub steel connection; finite element method; nonlinear analysis; genetic algorithm

Academic Editor: Raffaele Landolfo

Received: 27 November 2024
Revised: 18 December 2024
Accepted: 31 December 2024
Published: 2 January 2025

Citation: Grubits, P.; Balogh, T.; Movahedi Rad, M. Optimization of Bolted Steel T-Stub Connection Based on Nonlinear Finite Element Analysis Using Genetic Algorithm. *Infrastructures* **2025**, *10*, 8. https://doi.org/10.3390/infrastructures10010008

1. Introduction

Bolted connections are widely utilized for establishing steel structures due to their numerous advantages, such as streamlined construction and installation processes, making them particularly suited for modular designs [1,2], as well as their inherent reliability and durability [3,4]. Consequently, bolted steel joints are frequently utilized in bridge construction as part of significant infrastructure projects [5–8]. In the pursuit of complex designs, bolted steel connections are analyzed by discretizing the connection into a series of T-stub components, as represented in Figure 1. In this configuration, two T-shaped profiles are bolted together at their flanges, allowing the tensile load applied to the web to be transferred through flange bending and bolt tension.

A comprehensive understanding and accurate prediction of T-stub behavior are essential for determining the stiffness, strength, and ductility of joints. This can be achieved through analytical methods, such as the equivalent T-stub approach outlined in Eurocode [9]. However, these methods often lack the precision necessary for accurate analysis

due to the overall nonlinear behavior of these connections, which is influenced by numerous geometrical discontinuities, related stress concentrations, the presence of frictional forces, and the need to model uplift and contact forces [10]. To address these challenges, the finite element method (FEM) serves as a potential tool capable of capturing the complex behavior of T-stub elements [11].

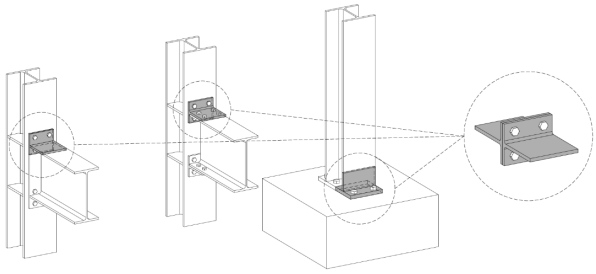

Figure 1. T-stub component in different steel joint scenarios.

As a result, numerous innovative applications of FEM have emerged for analyzing T-stub connections. An early example worth noting is the work of Bursi and Jaspart, who established a benchmark for FEM validation in modeling T-stub elements [12]. Furthermore, Neves et al. conducted a reliability analysis of T-stub components using FEM [13], while Al-Khatab and Bouchaïr examined the effects of strengthening backing plates, incorporating nonlinear material properties, contact interactions, and large deformations [14]. Another noteworthy development is the simplified finite element modeling for T-stub components, as demonstrated by Antonello et al. [15]. Recent studies have focused on the detailed analysis of T-stub elements fabricated from various steel materials, such as high-strength steel [16,17] and stainless steel [18], and assembled with different types of bolts [19]. Additionally, Jin et al. investigated an alternative T-stub configuration, where a circular tube is reinforced with a reverse-channel and secured using thread-fixed one-sided bolts [20].

Beyond the nonlinear behavior of the T-stub, a key challenge is designing for both strength and economic efficiency. This issue can be framed as a discrete structural optimization problem, which can be tackled using mathematical programming [21]. Recently, structural optimization has attracted significant attention from researchers across various steel design applications, including the optimization of trusses [22–25], beams [26–28], and connections [29,30] with the aim of reducing material usage and increasing stiffness.

To address the discrete mathematical problem of T-stub element design and ensure accurate analysis, this paper presents a comprehensive calculation framework that integrates genetic algorithm (GA) while considering nonlinear material, geometric, and contact properties. Unlike traditional code-based calculations, the proposed method enhances the precision of the analysis by utilizing FEM and performing a material and geometrical nonlinear analysis. However, this approach requires significant computational time due to the iterative nature of solving the complete loading history for the examined configurations. To overcome this limitation, an alternative modeling technique is proposed that significantly reduces the computation time while maintaining a high accuracy, providing a distinct advantage over the computationally intensive method commonly employed in other studies [12,16–18], where the connection components are modeled using solid FE elements. This method is applied during the optimization process, contributing to a more robust optimization by enabling the exploration of a wider range of configurations and refining the results more effectively.

To demonstrate the efficiency of the proposed framework, two different T-stub configurations, with and without bolt prestressing, were validated based on the work of Bursi

and Jaspart [12]. Subsequently, a comprehensive parameter sensitivity analysis was conducted to examine how different variables affect the structural behavior of the considered connection. Finally, optimization was performed to maximize the structural performance of the configuration. The results show that the proposed framework efficiently provides an optimal solution while reducing the simulation time through the use of the presented modeling technique.

2. Theoretical Foundations

This section provides a theoretical overview of the essential components of this research, including the key aspects of the nonlinear analysis and GA employed to develop the proposed design framework.

2.1. Nonlinear Analysis

To accurately represent the real-life behavior of steel structures, particularly bolted connections, it is essential to consider their nonlinear characteristics. However, a linear analysis is applicable when the displacements are sufficiently small, the material is linearly elastic, and the boundary conditions remain unchanged throughout the loading history [31]. Under these conditions, the equilibrium equation can be formulated as follows:

$$\boldsymbol{KU} = \boldsymbol{R} \tag{1}$$

where the displacement vector $\boldsymbol{U}$ is a linear function of the applied load $\boldsymbol{R}$, and the relationship between the two is defined by the global stiffness matrix $\boldsymbol{K}$.

The primary difficulty in nonlinear analysis lies in determining the global system's equilibrium state under applied forces. To address this issue, the external load is expressed as a function of time, allowing the equilibrium condition to be represented by the following equation:

$$\boldsymbol{R}^t - \boldsymbol{F}^t = 0 \tag{2}$$

where $\boldsymbol{R}^t$ represents the nodal forces exerted externally on the system at time t, while $\boldsymbol{F}^t$ indicates the internal nodal forces corresponding to the element stresses. By recognizing the existing stresses as the initial stresses, the following formula applies:

$$\boldsymbol{F}^t = \sum_i \int_{V_i^t} \boldsymbol{B}_i^t \sigma_i^t dV_i \tag{3}$$

where V_i represents the volume of element i, $\boldsymbol{B}$ is the finite element's strain–displacement matrix, and σ denotes the stress. When large deformations occur, the stresses and volumes of the elements become indeterminate; however, the system's equilibrium must be expressed in the current deformed geometry while adequately accounting for all nonlinearities throughout the complete load history. Consequently, the analysis of structures with nonlinear characteristics is performed incrementally, using specified step sizes. By considering an appropriate time interval Δt, the equilibrium condition at time $t + \Delta t$ is formulated as follows:

$$\boldsymbol{R}^{t+\Delta t} - \boldsymbol{F}^{t+\Delta t} = 0 \tag{4}$$

If the solution is determined at time t, the following equation is applied:

$$\boldsymbol{F}^{t+\Delta t} = \boldsymbol{F}^t + \boldsymbol{F} \tag{5}$$

where $\boldsymbol{F}$ represents the increase in internal forces resulting from the changes in element stresses and displacements from time t to time $t + \Delta t$. This variation can be determined

approximately by employing the tangent stiffness matrix $\boldsymbol{K}^t$, which accounts for the material and geometric conditions at time t. Consequently, the following formulas can be stated:

$$\boldsymbol{F} \cong \boldsymbol{K}^t \boldsymbol{U} \tag{6}$$

$$\boldsymbol{K}^t = \frac{\partial \boldsymbol{F}^t}{\partial \boldsymbol{U}^t} \tag{7}$$

where $\boldsymbol{U}^t$ is the nodal point displacement. By combining Equations (4)–(6), the following relationship is obtained:

$$\boldsymbol{K}^t \boldsymbol{U} = \boldsymbol{R}^{t+\Delta t} - \boldsymbol{F}^t \tag{8}$$

Finally, the displacement can be calculated approximately:

$$\boldsymbol{U}^{t+\Delta t} \cong \boldsymbol{U}^t + \boldsymbol{U} \tag{9}$$

During the finite element analysis, the well-known Newton–Raphson iteration method is utilized as a solution technique, enabling the effective resolution of nonlinear problems, such as elastic–plastic material behavior, large deformations, and contact interactions between different components.

During static analysis, where time does not influence the system's behavior, it serves merely as a convenient variable corresponding to different load intensities; thus, t can be interpreted as a load factor.

2.2. Genetic Algorithm

The genetic algorithm (GA) is a widely utilized heuristic approach among various optimization techniques, valued for its flexibility in addressing a broad range of practical problems [32]. Moreover, GA is particularly effective for nonlinear optimization tasks, as its operating principle allows it to adapt to large search spaces, avoid convergence to local minima, and eliminate reliance on an assumed starting model. Consequently, this algorithm is highly suitable for addressing various structural optimization problems [33–36].

The core principle of GA is to generate a set of candidate solutions, with each member representing a potential optimal solution to the optimization problem. Throughout the optimization process, GA simulates natural evolution to maximize or minimize the objective function, which corresponds to the fitness function [37]. As a result, the fitness function evaluates the quality of the solutions and plays a crucial role in shaping the entire optimization process.

Another key component of GA is the chromosome, which encodes the solution and contains all the characteristics under evaluation. In this research, a standard bit-string representation is used to construct chromosomes, consisting of a random combination of zeros and ones. At the beginning of the optimization process, the initial population is randomly generated, producing a variety of chromosomes, and the fitness value is calculated for each individual. Subsequently, genetic operators, including crossover, mutation, and selection, are applied to iteratively search for the optimal solution until convergence is achieved over several generations.

The crossover operator is responsible for combining the chromosomes of selected solutions [38], where two or more parents are chosen based on the fitness value, and their genetic codes are merged. For standard bit-string-based chromosomes, an n-point crossover can be employed, which divides the genetic code of two parents into n segments and alternately assembles them to form a new chromosome [32], thereby creating the offspring. Another widely recognized method is uniform crossover, which generates two offspring from two parents. In this case, two outcomes are possible: either the offspring are

identical to the parents, or bits are randomly selected from the chromosomes of the parents. This process is governed by the crossover probability, which dictates the likelihood of each scenario occurring [39].

To conduct the crossover procedure, a mating pool must be created, containing the potential parents for the next generation [40]. Various selection methods can be employed for this purpose, such as the well-known tournament selection. The fundamental concept involves organizing a tournament among N competitors, where N represents the tournament size, and the winner is determined based on the lowest or highest fitness value [41]. Subsequently, the winner is added to the mating pool until it is filled.

The next key operator in GA is the mutation procedure. During this phase, the chromosome is randomly altered by the operator, with the extent of alteration determined by the mutation rate. With the help of these operators, a new generation is created, and the fitness values of the individuals are calculated once again. This process continues until the final predefined generation is reached or the convergence criteria are satisfied.

3. Finite Element Modeling

This section presents the finite element models of the selected T-stub connections, validated using ABAQUS [42] software, with reference to the work of Bursi and Jaspart [12]. Two distinct modeling techniques are also introduced. To demonstrate the effectiveness and potential for industrial applications of the alternate modeling technique, the validation of the first T-stub setup was performed using AXISVM as well [43], a commercial finite element software widely utilized in advanced industrial engineering. Finally, a parameter sensitivity analysis was conducted to investigate how various parameters influence the structural behavior of the T-stub connection, and to further demonstrate that the results obtained using the alternative modeling technique are in close agreement with those from the initially developed FE model.

3.1. Finite Element Model

In this section, a finite element model of the T-stub bolted connection was developed based on the work of Bursi and Jaspart [12], as shown in Figure 2, which accurately represents the specimens used in the experiments, including all their geometric parameters. Subsequently, two setups were validated using ABAQUS software: one with regular bolts and the other with preloaded bolts.

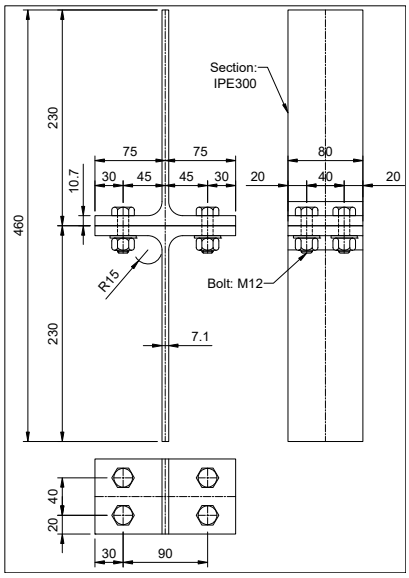

Figure 2. Configuration of the considered bolted T-stub.

To develop the model of the T-stub configuration, IPE300 sections and bolt components were modeled using 8-node linear brick elements with reduced integration (C3D8R) and hexahedral element shapes. The general mesh size for the sections was set to 5 mm, while a mesh size of 2 mm was applied for the bolts, as illustrated in Figure 3, which also shows the boundary and load conditions. A displacement-controlled analysis was performed, with external loads applied through imposed displacements, corresponding to the experimental test setup.

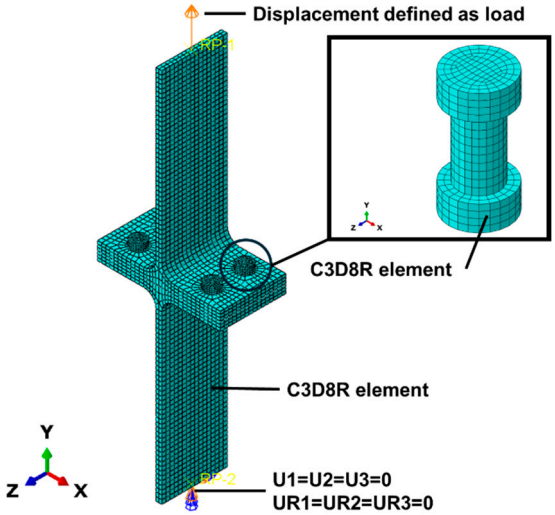

Figure 3. Finite element model of the considered T-stub connection.

To enhance the precision of the analysis and capture the actual structural behavior, an elastic–plastic material model of steel with isotropic hardening was employed, based on experimental tests. The material properties for the flange, web, and bolts were defined separately. The true stress–strain relationships, as reported in [12], are illustrated in Figure 4, with the key characteristics summarized as follows:

- Flange: elasticity modulus $E = 240,782$ N/mm^2, yield stress $f_y = 431$ N/mm^2, and ultimate tensile stress $f_u = 787$ N/mm^2;
- Web: elasticity modulus $E = 217,130$ N/mm^2, yield stress $f_y = 469$ N/mm^2, and ultimate tensile stress $f_u = 787$ N/mm^2;
- Bolt: elasticity modulus $E = 160,612$ N/mm^2, yield stress $f_y = 893$ N/mm^2, and ultimate tensile stress $f_u = 1025$ N/mm^2.

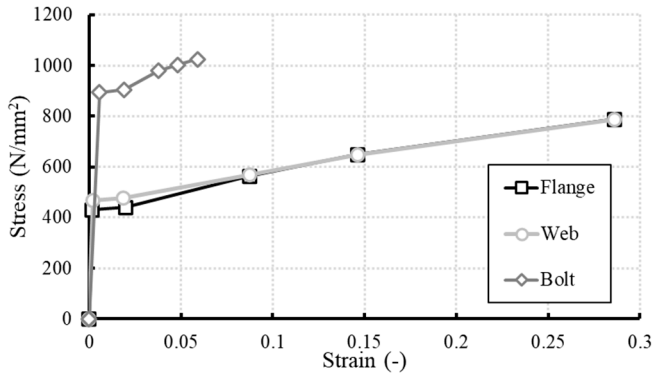

Figure 4. Stress–strain relationship of the steel materials used in the analysis.

In modeling steel bolted connections, simulating friction interactions between different parts of the assembly is crucial. This was achieved using a "surface-to-surface" contact

approach, where a penalty formulation was employed for tangential behavior with a friction coefficient of 0.3, and "hard" contact was utilized for normal behavior.

As mentioned previously, two configurations were modeled: one with regular bolts and the other with preloaded bolts. In the model incorporating solid brick elements, the first configuration is referred to as T1_NPL_SO, while the second is designated as T1_PL_SO. A bolt load of $R_{p0} = 78.91$ kN was applied to verify the behavior of T1_PL_SO. In this case, the bolts were first preloaded, and then the ultimate displacement was imposed on the overall configuration.

The simulation was conducted using the Newton–Raphson iteration method, incorporating the effects of large deformation. Upon completion of the analysis, the force–displacement relationship of the connection was compared to the experimental results presented in the research by Bursi and Jaspart [12]. The outcomes are illustrated in Figure 5, showing a close agreement between the numerical and experimental results. Additionally, the design resistance in tension of the proposed setup was calculated in accordance with EN 1993-1-8, assuming Mode 2 failure, characterized by the simultaneous fracture of bolts and flange yielding [9]. It is worth noting that this method is one of the most commonly used approaches in engineering design practice, particularly for complex connections that are otherwise difficult to analyze. The calculated plastic tension resistance shows good agreement with the numerical results, as presented in Figure 5. However, it should be acknowledged that this method involves certain simplifications, such as neglecting the strain-hardening effect. In contrast, the numerical solution offers greater precision and facilitates the analysis of more complex behaviors.

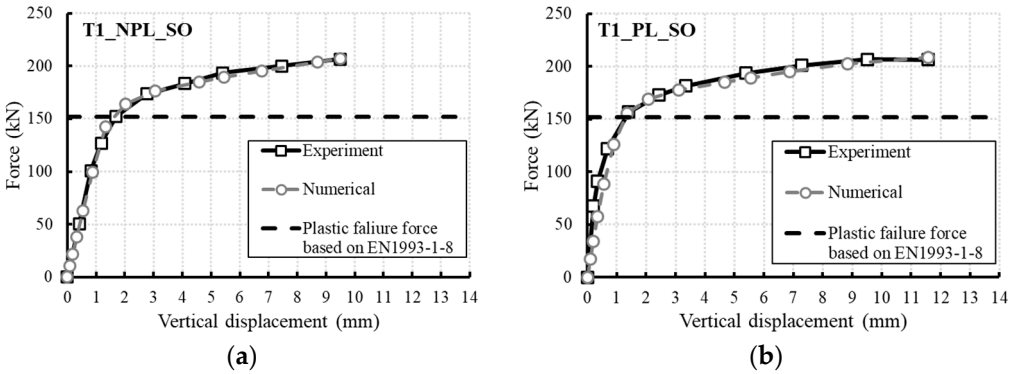

Figure 5. The force–displacement relationship of the T-stub connection: (**a**) without preload, and (**b**) with preload [9].

For a more detailed analysis, the initial stiffness values, representing the elastic phase of the configuration, were calculated and compared for both the experimental test and the numerical model, based on the slope of the linear portion of the force–displacement curves. The results are presented in Table 1, along with the ultimate force values corresponding to the displacement defined as the load. The deviation values in Table 1 are calculated as the difference between the numerical and experimental values, expressed as a percentage of the experimental value. This provides a normalized measure of how closely the numerical model approximates the experimental results, enabling a direct comparison of the model's accuracy. This analysis further demonstrates that the numerical outcomes closely match the experimental data, with the deviations in both initial stiffness and ultimate force remaining below 5% for this modeling approach. Considering previous studies [44,45], these deviations fall within an acceptable error range, which can be up to 10%.

Table 1. Comparison of experimental and numerical results for the detailed finite element model.

Configuration	Initial Stiffness (N/mm)		Deviation (%)	Ultimate Force (kN)		Deviation (%)
	Experimental $k_{i,exp}$	Numerical $k_{i,num}$	$k_{i,num} - k_{i,exp} / k_{i,exp}$	Experimental $R_{u,exp}$	Numerical $R_{u,num}$	$R_{u,num} - R_{u,exp} / R_{u,exp}$
T1_NPL_SO	108,082	106,755	−1.23%	206.59	207.07	−0.23%
T1_PL_SO	110,743	114,698	3.57%	206.32	208.62	1.11%

3.2. Alternate Finite Element Model

In this section, an alternative modeling technique that reduces the simulation time and computational demand, while ensuring that the results deviate only marginally from those of the model described previously, is presented. This approach proved especially useful during the optimization process, significantly shortening its duration.

To maintain the precision of the outcomes and reduce computational demand, hexahedral 4-node shell elements (S4R) were used to model the IPE300 sections of the T-stub connection instead of C3D8R elements, resulting in a reduction in the overall number of elements. Additionally, the bolts were modeled using 2-node linear beam elements for the shank, while the S4R elements were used for the bolt heads. A coupling constraint was applied between the two components to ensure a proper connection. In both cases, the same mesh size was applied as mentioned in the previous section. The developed FE model is presented in Figure 6.

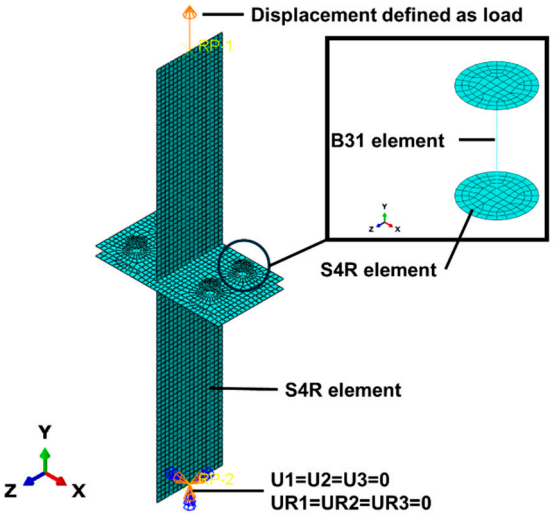

Figure 6. Alternate finite element model of the considered T-stub connection.

During the simulation, the same material model, contact properties, and pretension forces were employed. In this case, the model with regular bolts is designated as T1_NPL_SH, while the assembly with a preload is designated as T1_PL_SH. The results of the analysis are presented in Figure 7, again demonstrating a close agreement with the experimental test.

Once again, the obtained initial stiffness and ultimate force values were compared, as shown in Table 2. Notably, the deviations between the examined parameters changed only slightly, compared to the previous modeling technique. Additionally, the simulation time could be significantly reduced in this case, as presented in Table 3, further demonstrating the effectiveness of this modeling method.

The proposed modeling technique not only reduces the simulation time without compromising the precision of the analysis but is also suitable for other software commonly preferred in industrial design situations. To demonstrate this, AXISVM—a well-known

finite element software in industrial engineering applications—was utilized to recreate the T-stub connection. The results from the T1_NPL_SH case were compared to the experimental test again.

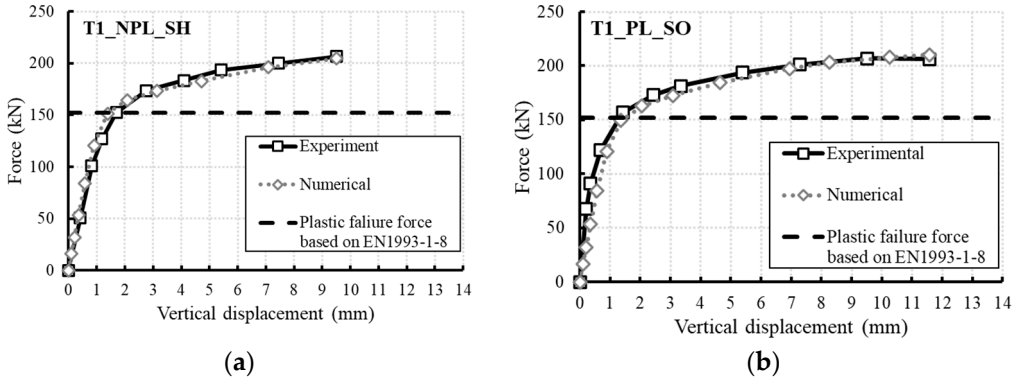

Figure 7. Force–displacement relationship of the T-stub connection using the alternative modeling technique: (**a**) without preload; and (**b**) with preload [9].

Table 2. Comparison of experimental and numerical results for the alternative finite element model.

Configuration	Initial Stiffness (N/mm)		Deviation (%)	Ultimate Force (kN)		Deviation (%)
	Experimental $k_{i,exp}$	Numerical $k_{i,num}$	$k_{i,num} - k_{i,exp} / k_{i,exp}$	Experimental $R_{u,exp}$	Numerical $R_{u,num}$	$R_{u,num} - R_{u,exp} / R_{u,exp}$
T1_NPL_SH	108,082	109,773	1.57%	206.59	204.60	−1.02%
T1_PL_SH	110,743	110,378	−0.33%	206.32	210.15	1.85%

Table 3. The CPU time required for the simulation.

T1_NPL_SO	T1_NPL_SH	T1_NPL_SO	T1_PL_SH
198 s	96 s	259 s	99 s

In the AXISVM software, triangular shell elements are employed for the sections and bolt heads to capture the nonlinear material behavior of steel. The shank of the bolt is modeled using beam elements. The general mesh size for all elements aligns with the value specified earlier in this study.

During the simulation, the same yield strength and ultimate tensile strength, as presented in Figure 4, were utilized, applying the von Mises yield criterion and an isotropic linear hardening rule. This approach is also recommended by Eurocode for design situations where material properties are treated as nominal [46].

To simulate the contact between the parts of the T-stub connection, "gap" elements were used. This solution has an inactive state characterized by a small stiffness value, representing the phase when no contact is achieved, and an active state with a stiffness value several orders of magnitude higher, indicating when contact is established [43]. This element is used between two points; therefore, in the assembly, it was defined at discrete locations, as shown in Figure 8, which illustrates the developed finite element model in the AXISVM software.

During the simulation, large displacements were considered, and the load was applied in the form of force. Therefore, a force-controlled analysis was conducted using the Newton–Raphson method and the same boundary conditions presented previously. The results, once again, showed good agreement with the experimental test, as illustrated in Figure 9, demonstrating the applicability of the methodology to software designed primarily for practical engineering applications.

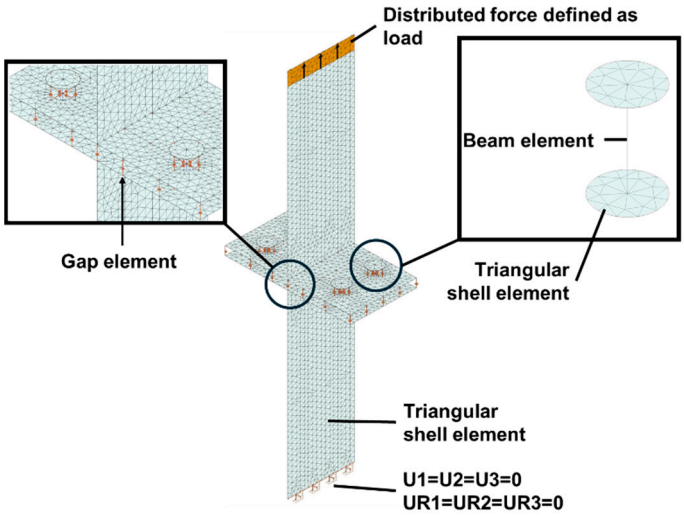

Figure 8. The developed finite element model in AXISVM.

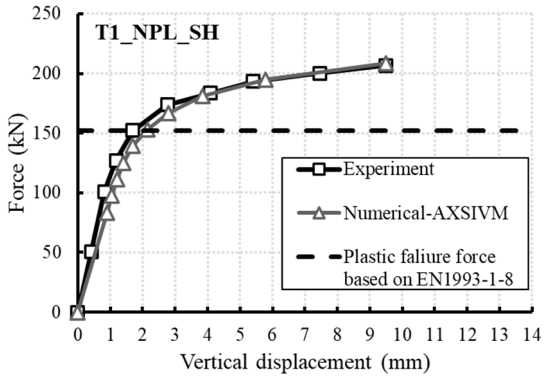

Figure 9. Comparison between the force–displacement relationship for the T1_NPL_SH configuration using AXISVM software for simulation [9].

3.3. Parameter Sensitivity Analysis

In this section, a sensitivity analysis is conducted to examine the influence of various parameters on structural behavior. It is important to note that the primary objective of this paper is to present an effective optimization framework to maximize the performance of T-stub connections. Therefore, this section focuses on demonstrating the range of possible outcomes and further verifying the accuracy of the alternative modeling technique by comparing the simulation results with those obtained from the initial FE model. The analysis considers the following parameters:

- Size of cross-section of T-stub element: IPE180, IPE220, IPE270, IPE330, IPE360.
- Type of bolts: M16, M18, M20.
- Axial distance between bolts in transverse direction: 70 mm, 80 mm, 100 mm, 110 mm.
- Prestressing force of bolts: $0.8R_{p0} = 63.12$ kN, $0.9R_{p0} = 63.12$ kN, $1.1R_{p0} = 86.80$ kN, $1.2\ R_{p0} = 94.73$ kN, $1.3\ R_{p0} = 102.58$ kN.

In this section, the notation "SO" refers to the FE models constructed using 3D brick elements, representing the initial modeling technique, while "SH" denotes the alternative modeling technique, which employs shell elements to represent the T-stub configurations.

The first parameter investigated was the size of the cross-section of the T-stub elements, which was varied as presented in the previous list. To create models corresponding to the specified cross-sections, the thickness of the flange and web plates, as well as the root radius, were adjusted in accordance with the Eurocode standards. The results are shown in Figure 10, where it can be observed that the performance of both configurations improves

with the increase in section size, as expected. However, when considering the prestressing force of the bolts, the ultimate load does not significantly increase beyond the IPE270 section. A closer examination reveals that this phenomenon occurs due to the increased yielding of the prestressed bolts. The combination of prestressed bolts and large flange thickness shifts the connection's failure mode toward Mode 3, where the dominant failure mechanism is bolt fracture [9], resulting in a greater plastic deformation of the bolts. In contrast, for smaller cross-sections, the plastic zone primarily develops in the flange, with a moderate plasticity observed in the bolts. Furthermore, the results of the two modeling techniques demonstrate good agreement. The obtained initial stiffness and ultimate load values are summarized in Table 4.

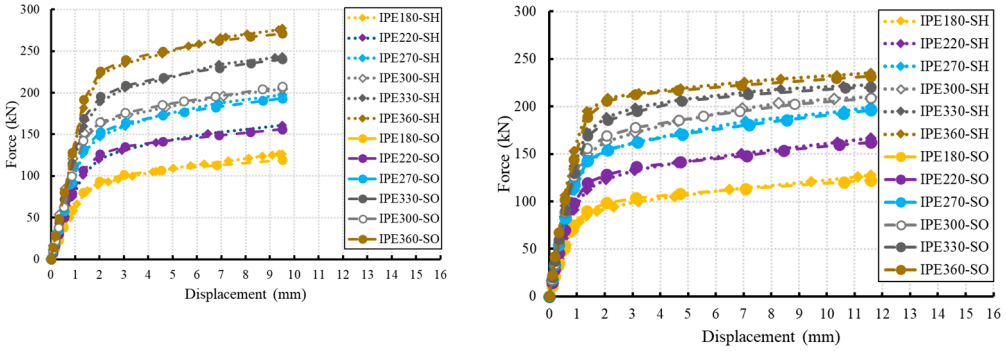

(**a**) (**b**)

Figure 10. Effect of cross-section size on the structural behavior of the configurations: (**a**) without bolt preload, and (**b**) with bolt preload.

Table 4. Initial stiffness and ultimate force values for the two modeling techniques considering different cross-sectional sizes of T-stub elements.

Cross-Section	Initial Stiffness (N/mm)				Ultimate Force (kN)			
	Without Preload		With Preload		Without Preload		With Preload	
	Initial Model	Alternate Model	Initial Model	Alternate Model	Initial Model	Alternate Model	Initial Model	Alternate Model
IPE180	61,013	61,999	66,193	63,516	119.12	126.62	122.23	127.44
IPE220	80,358	84,146	87,523	82,927	156.00	160.85	162.04	166.50
IPE270	98,814	103,403	103,078	102,948	193.35	197.70	196.00	199.42
IPE300	106,755	109,773	114,698	110,378	207.07	204.60	208.62	210.15
IPE330	126,078	128,539	121,912	126,680	240.12	243.49	220.18	223.02
IPE330	142,462	143,577	137,989	143,439	270.97	277.35	231.63	235.21

The next parameter investigated is the type of bolts, which includes M16, M18, and M20, in accordance with the Eurocode standard. The results are presented in Figure 11. For both configurations, the bolts influence the structural behavior in a similar manner, consistently leading to an increase in initial stiffness and ultimate load, as expected. Once again, the results from the alternative modeling technique show good agreement with the outcomes obtained from the FE models constructed using 3D brick elements, further supported by the data in Table 5.

As part of the sensitivity analysis, the effect of the bolt's axial distance in the transverse direction was investigated. Reducing the transverse spacing of the bolts adversely impacts the structural performance of the connection. This occurs because a greater distance between the bolts and the resultant load amplifies the moment-induced stress in the bolts. As illustrated in Figure 12, this has a significant effect on the ultimate force, similar to the impact of increasing the bolt diameter. The results in Table 6 further highlight the significance of bolt positioning on

both the initial stiffness and ultimate force. Furthermore, the outcomes from the two modeling techniques show good agreement with each other in this case as well.

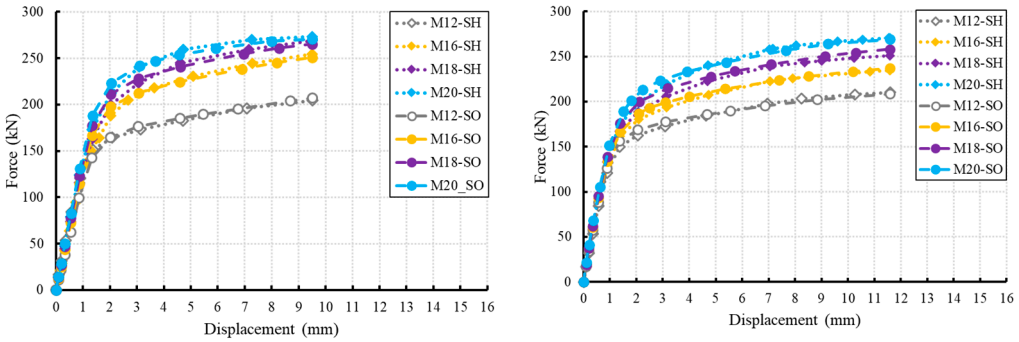

(**a**) (**b**)

Figure 11. Effect of bolt type on the structural behavior of the configurations: (**a**) without bolt preload, and (**b**) with bolt preload.

Table 5. Initial stiffness and ultimate force values for the two modeling techniques considering different types of bolts.

Bolt	Initial Stiffness (N/mm)				Ultimate Force (kN)			
	Without Preload		With Preload		Without Preload		With Preload	
	Initial Model	Alternate Model	Initial Model	Alternate Model	Initial Model	Alternate Model	Initial Model	Alternate Model
M12	106,755	109,773	114,698	110,378	207.07	204.60	208.62	210.15
M16	124,364	124,187	120,754	117,445	250.99	254.43	236.98	234.59
M18	131,716	133,286	127,156	122,467	265.35	268.58	258.13	251.08
M20	138,532	141,358	125,600	127,395	270.51	273.07	269.00	270.26

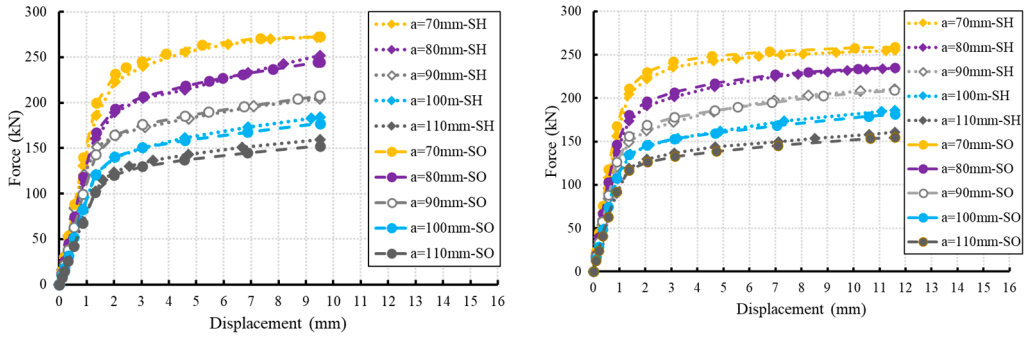

(**a**) (**b**)

Figure 12. Effect of bolt axial distance in transverse direction on the structural behavior of the configurations: (**a**) without bolt preload, and (**b**) with bolt preload.

Finally, the effect of the prestressing force was evaluated for the previously proposed T-stub configuration, considering the bolt preload. As shown in Figure 13, the magnitude of the preload has a smaller influence on the ultimate load of the connection compared to the previously investigated parameters. However, if the preload drops below a certain threshold, it may lead to a reduction in structural performance. Furthermore, the initial stiffness of the connection is not significantly affected. In this case as well, the results obtained from the two different modeling techniques show good agreement, as summarized in Table 7.

Table 6. Initial stiffness and ultimate force values for the two modeling techniques considering different axial distances in transverse direction between bolts.

Axial Distance in Transverse Direction Between Bolts	Initial Stiffness (N/mm)				Ultimate Force (kN)			
	Without Preload		With preload		Without Preload		With Preload	
	Initial Model	Alternate Model	Initial Model	Alternate Model	Initial Model	Alternate Model	Initial Model	Alternate Model
70 mm	147,306	149,167	155,483	150,516	272.73	272.11	259.00	255.11
80 mm	124,449	129,995	132,389	127,298	244.87	251.78	235.35	234.58
90 mm	106,755	109,773	114,698	110,378	207.07	204.60	208.62	210.15
100 mm	91,268	90,833	98,934	95,912	177.04	184.38	181.20	185.73
110 mm	76,999	77,283	85,549	87,617	152.52	159.46	154.78	160.59

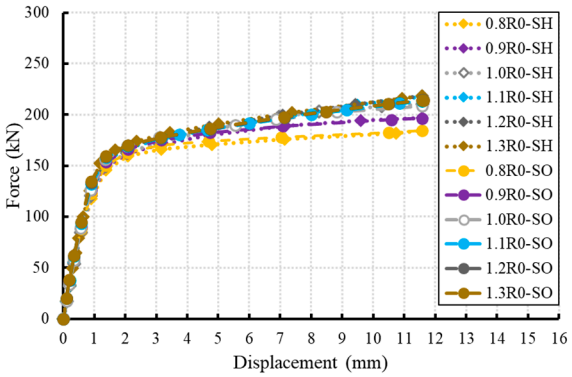

Figure 13. Effect of prestressing force of bolts on the structural behavior of the configurations with bolt preload.

Table 7. Initial stiffness and ultimate force values for the two modeling techniques considering different bolt prestressing forces.

Prestressing Force	Initial Stiffness (N/mm)		Ultimate Force (kN)	
	Initial Model	Alternate Model	Initial Model	Alternate Model
$0.8R_{p0}$	109,578	106,431	184.42	184.52
$0.9R_{p0}$	111,874	108,863	196.45	197.10
$1.0R_{p0}$	114,698	110,378	208.62	210.15
$1.1R_{p0}$	115,055	113,099	213.37	217.85
$1.2R_{p0}$	116,128	114,530	214.37	218.80
$1.3R_{p0}$	116,323	120,161	214.10	218.60

In general, the results of the parameter analysis reveal a wide range of possible outcomes, highlighting the importance of applying optimization algorithms. This is particularly evident in the case of bolt positioning, as the relationship between bolt positions and structural performance can lead to significant improvements without requiring additional material, such as larger section sizes or bolt diameters. Consequently, this approach can contribute to a more economically efficient design. Therefore, in this paper, the optimization framework is specifically designed to determine the ideal bolt layout, along with their appropriate prestressing values.

4. Optimization Process

This section presents the optimization framework, which is the main focus of the study, based on FEM and utilizing GA. The results of the process are then presented and discussed.

4.1. Problem Formulation and Optimization Framework

During the design process of a steel connection, the position of the bolts can significantly influence the overall stiffness of the joint [47]. This observation is supported by the results of the parameter sensitivity analysis, where the influence of the axial distance between bolts was investigated. Additionally, finding the optimal layout to maximize structural performance can be challenging. Therefore, in this part of the study, GA developed using PYTHON programming language was integrated with ABAQUS software to determine the ideal positions and prestressing force of the bolts.

The primary objective was to achieve the highest possible mechanical performance by enhancing both the stiffness and the ultimate load-bearing capacity of the joint. However, it is important to note that during structural design, several other criteria must also be considered and satisfied, such as deformation and plastic strain limitations [48], as well as various detailing rules. In this research, the regularization of bolt positions and the prestressing force were considered as optimization constraints, as presented later in this section.

To evaluate the structural performance of the previously presented configurations, the objective function, also known as the fitness function and denoted as $\boldsymbol{f}$, was formulated based on the stiffness of the connection and the ultimate force value. Consequently, the stiffness, defined as the ratio of the applied force $\boldsymbol{R}$ to the displacement $\boldsymbol{U}$, was calculated for each Δt increment throughout the overall loading history and summarized at the end of the simulation. Additionally, the ultimate force $\boldsymbol{R}_u$ at the final increment was incorporated into the fitness function, alongside the incremental stiffness terms, to determine the fitness number.

In the optimization process, a displacement constraint was imposed, requiring that the displacement at the load level $\boldsymbol{R}_{ult}$ meets or exceeds the specified ultimate displacement $\boldsymbol{U}_{ult}$ for the design. Additionally, the Eurocode guidelines for bolt positioning and preload were incorporated into the optimization framework to maintain compliance with design standards [9]. In this manner, the optimization problem can be formulated as follows:

$$maximize \ : \ \boldsymbol{f} = \boldsymbol{R}_u + \sum_{i=1} \frac{\boldsymbol{R}^{t_i+\Delta t} - \boldsymbol{R}^{t_i}}{\boldsymbol{U}^{t_i+\Delta t} - \boldsymbol{U}^{t_i}} \tag{10}$$

$$Subject\ to: \ \sum_{i=1} (\boldsymbol{U}^{t_i} - \boldsymbol{U}^{t_i+\Delta t}) \geq \boldsymbol{U}_{ult} \tag{11}$$

$$e \geq 1.2d \tag{12}$$

$$p \geq 2.4d \tag{13}$$

$$R_p \leq \ 0.7 f_{ub} \frac{d^2 \pi}{4} \tag{14}$$

$$t_{i+1} = t_i + \Delta t, \ where: \ i \in \mathbb{Z} \tag{15}$$

where i represents the current iteration number, e denotes the edge distance from the center of the bolt hole, p is the spacing between bolt centers, R_p is the bolt preload value, f_{ub} represents the ultimate tensile strength of the bolts, and d is the nominal bolt diameter.

During the optimization process, the design domain was defined based on the constraints represented by Equations (12)–(14). Accordingly, the distance between bolts in the transverse direction was allowed to vary between 57 mm and 120 mm in 1.00 mm discrete steps, while in the longitudinal direction, it ranged from 26 mm to 50 mm in 0.75 mm discrete steps. Additionally, the bolt prestressing force was allowed to range between 0 kN and the optimal prestressing value, as specified by Eurocode [9]: $\mathrm{R_p} = 0.7\mathrm{f_{ub}}\frac{\mathrm{d}^2\pi}{4}$.

The optimization process was implemented using the PYTHON programming language to develop GA, which was integrated with the ABAQUS software to calculate the

fitness value of each individual, based on the mechanical properties. This was achieved by creating a comprehensive PYTHON script that encapsulates all of the key aspects of the proposed FEM model parametrically. During the optimization, a standard bit-string chromosome was used to represent different bolt layouts and prestressing forces. After generating a population, the developed program decodes the chromosomes for ABAQUS, filling predefined parameters with values, and resulting in the creation of individual models. Subsequently, the simulation is conducted, and an additional part of the code processes the results and calculates the fitness based on Equation (10).

Once the fitness value is determined, the aforementioned genetic operators, which are also included in the developed PYTHON program, generate offspring. This process continues until the final generation is reached. The framework is illustrated in Figure 14. During optimization, the previously presented alternative modeling technique is used to reduce computational time, significantly shortening the overall process duration.

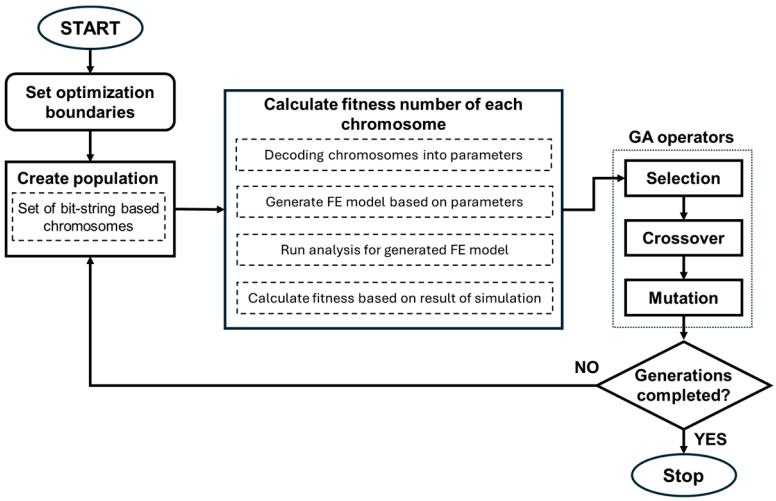

Figure 14. Optimization framework based on FEM and GA.

Before starting the optimization, the key characteristics of the GA needed to be defined. In this study, the population size was set to 50, which is a commonly used value in similar optimization problems [35], as it strikes a balance between computational efficiency and solution diversity.

To create the mating pool, tournament selection, as described earlier in this paper, was used due to its simplicity and effectiveness [49], with a tournament size of 2. In this case, the individual with the better fitness between the two competitors is selected as the winner. This tournament size has been shown to improve the likelihood of identifying the global optimum by promoting diversity in the mating pool [50].

Subsequently, a crossover was performed using the uniform crossover method, as previously introduced in this paper, with a crossover probability of 0.7. By setting the probability to this value, the algorithm strikes a balance between exploration and exploitation, allowing for a reasonable amount of exploration without excessively disrupting the existing solutions. This helps maintain convergence toward the global optimum, as demonstrated in other studies [25].

Finally, the mutation process involved flipping bits at random positions, governed by the mutation probability. Initially, the mutation probability was set to 0.1 and gradually increased with each generation, reaching 0.9 in the final generation. This approach allows the algorithm to explore a broader solution space, improving the chances of finding the global optimum [51], and has been used by other researchers [34] to improve the optimization process. Additionally, an elitist operator was incorporated, ensuring that the two

best solutions from each generation were carried over directly to the next. This strategy is commonly used to maintain solution quality and has proven to be an effective tool during optimization [25].

4.2. Results and Discussion

This section presents the optimization results. The proposed outcomes demonstrate the efficiency of the developed framework, which is capable of finding an optimal solution in a reduced amount of time due to the use of the previously introduced alternative modeling technique.

The optimization history presented in Figure 15 shows that the convergence of the maximum fitness values was achieved in the third generation. Additionally, the average values began to stabilize after the fourth generation, remaining within a relatively narrow range.

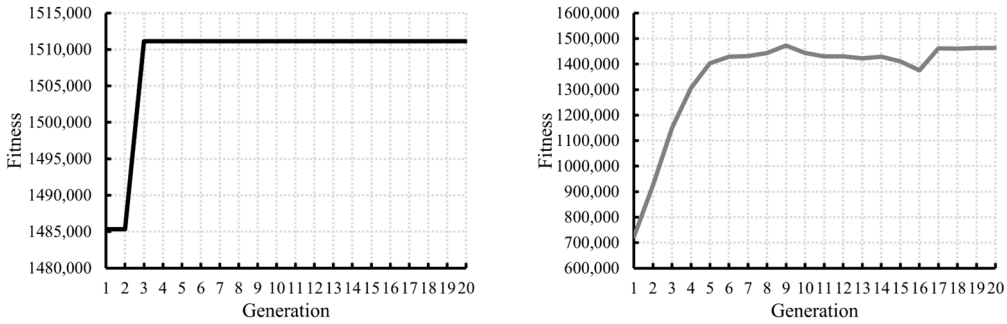

Figure 15. Evolution history of fitness function: (**a**) maximum values and (**b**) average values.

Upon completion of the optimization, the best and worst individuals, based on the calculated fitness values, were compared to the validated numerical model T1_PL_SH. The proposed framework led to a significant improvement in structural performance, as shown in Figure 16. A further analysis revealed a 50.2% increase in initial stiffness, compared to the original configuration, along with a 30.6% improvement in ultimate force. These values are presented in Table 8, and the optimal layout of bolts are presented in Figure 17, where the boundaries of the bolt positions are marked based on Eurocode. The optimal prestressing force obtained through the process matched the value specified by Eurocode: $R_p = 0.7\, f_{ub} \frac{d^2 \pi}{4}$. These results demonstrate that the proposed optimization framework holds significant potential for achieving cost-effective designs, even in the case of large design spaces and nonlinear optimization problems, due to the use of GA, which bypasses the reliance on an assumed starting model.

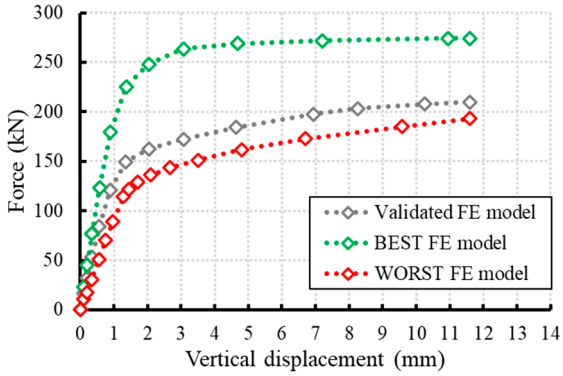

Figure 16. Comparison of the force–displacement relationship between the validated numerical model and the best and worst configurations obtained through the optimization process.

Table 8. Comparison of the validated numerical model with the best and worst configurations obtained through the optimization process.

Model	Initial Stiffness	Deviation	Ultimate Force	Deviation
Validated	$k_{i,V} = 110,378$ N/mm	–	$R_{u,V} = 209.88$ kN	–
BEST	$k_{i,B} = 165,743$ N/mm	$\frac{k_{i,B}-k_{i,V}}{k_{i,V}} = 50.2\%$	$R_{u,B} = 274.13$ kN	$\frac{R_{u,B}-R_{i,V}}{R_{i,V}} = 30.6\%$
WORST	$k_{i,W} = 89,402$ N/mm	$\frac{k_{i,W}-k_{i,V}}{k_{i,V}} = -19.0\%$	$R_{u,W} = 193.15$ kN	$\frac{R_{u,W}-R_{i,V}}{R_{i,V}} - 8.0\%$

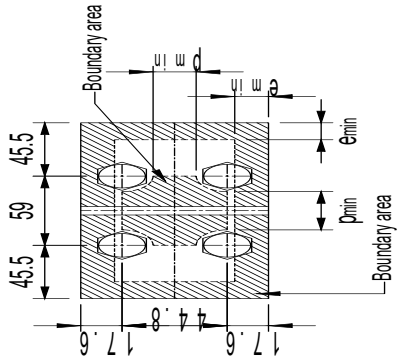

Figure 17. Optimal bolt layout obtained through the optimization process.

During the optimization process, plastic strains were not directly minimized, as shown in Equation (10); however, the values were analyzed for further examination. Notably, the maximum plastic strain was also reduced through the optimal distribution of bolts and prestressing force, as illustrated in Figure 18.

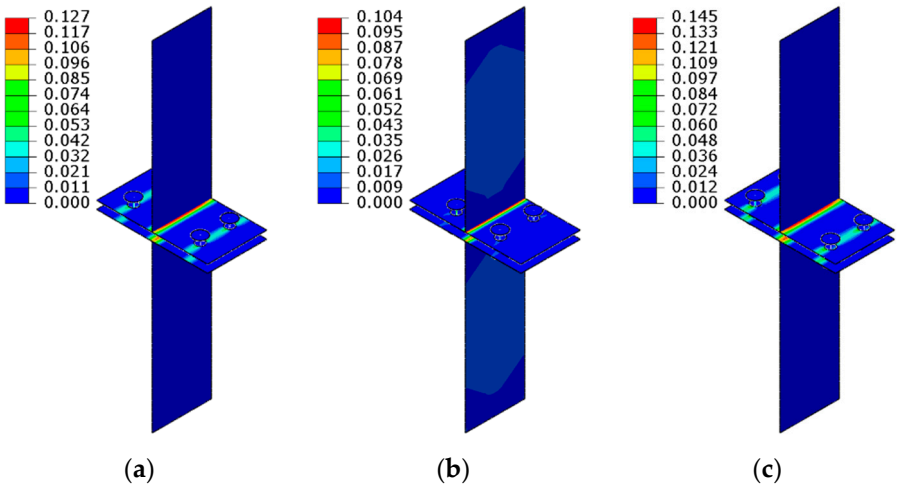

Figure 18. Resulting plastic strain values for (**a**) the validated numerical model, (**b**) the best configuration, and (**c**) the worst configuration.

5. Conclusions

This paper presents an optimization framework developed to enhance the structural performance of T-stub connections by accounting for the elasto-plastic properties of steel, large displacements, and contact interactions between components. The framework addresses the complexities of steel connection design, such as the reliance on numerous discrete variables, while ensuring precise analysis through the incorporation of nonlinear behavior. To demonstrate the effectiveness of the proposed approach, the optimal bolt layout and prestressing force for a selected T-stub connection were determined, and the structural performance was compared to the initial configuration.

The introduced framework was developed using the finite element method (FEM), ensuring precision by conducting a material and geometrical nonlinear analysis, including nonlinear contacts. Two T-stub configurations were validated against experimental tests. An alternative modeling technique was also introduced to reduce the computational time without significantly affecting the simulation accuracy, making the optimization process more efficient. Furthermore, this modeling method is compatible with software commonly used in industrial design applications. This was demonstrated using AXISVM software, which is widely utilized in advanced industrial engineering.

Genetic algorithm (GA) was employed to optimize the selected T-stub configuration, developed using the PYTHON programming language. The objective function aimed to maximize structural performance, with the fitness value calculated based on the connection's ultimate force and stiffness, while adhering to Eurocode design requirements for bolt positioning and prestressing force. Genetic operators were applied to improve the probability of identifying the global optimum solution.

The results demonstrated the effectiveness of the developed framework. By applying the proposed methodology, the initial stiffness of the T-stub connection was improved by 50.2%, and the ultimate force increased by 30.6%, compared to the validated initial configuration, through the optimization of the bolt layout and prestressing forces. Consequently, these results verify the potential of the proposed optimization framework in steel connection design and highlight its capability to be extended for optimizing more complex configurations.

Author Contributions: Writing—original draft, investigation, visualization, software, validation, coding, P.G.; conceptualization, methodology, software, writing—review and editing, supervision, M.M.R.; supervision, validation, writing—review and editing, T.B. All authors have read and agreed to the published version of the manuscript.

Funding: This project was implemented with the support provided by the Ministry of Culture and Innovation of Hungary from the National Research, Development and Innovation Fund, financed under the University Research Scholarship Programme EKÖP-2024.

Data Availability Statement: The authors confirm that the supporting data for this study's conclusions are included in the publication.

Conflicts of Interest: Tamás Balogh is employed by Inter-CAD Ltd., and other authors declare no conflicts of interest.

References

1. Lacey, A.W.; Chen, W.; Hao, H.; Bi, K. Review of Bolted Inter-Module Connections in Modular Steel Buildings. *J. Build. Eng.* **2019**, *23*, 207–219. [CrossRef]
2. Zhai, S.Y.; Lyu, Y.F.; Cao, K.; Li, G.Q.; Wang, W.Y.; Chen, C. Seismic Behavior of an Innovative Bolted Connection with Dual-Slot Hole for Modular Steel Buildings. *Eng. Struct.* **2023**, *279*, 115619. [CrossRef]
3. Ribeiro, T.; Bernardo, L.; Carrazedo, R.; De Domenico, D. Seismic Design of Bolted Connections in Steel Structures—A Critical Assessment of Practice and Research. *Buildings* **2022**, *12*, 32. [CrossRef]
4. Yang, B.; Tan, K.H. Experimental Tests of Different Types of Bolted Steel Beam-Column Joints under a Central-Column-Removal Scenario. *Eng. Struct.* **2013**, *54*, 112–130. [CrossRef]
5. Xu, G.; Wang, Y.; Du, Y.; Zhao, W.; Wang, L. Static Strength of Friction-Type High-Strength Bolted T-Stub Connections under Shear and Compression. *Appl. Sci.* **2020**, *10*, 3600. [CrossRef]
6. Zhang, Y.; Zhan, J.; Liao, Y.; Ding, W.; Tan, S.; Liu, Y. Experimental and Numerical Studies on Hybrid Bolted Connection of Steel Box Girders: Bending Mechanism. *Eng. Struct.* **2024**, *321*, 118986. [CrossRef]
7. Liu, X.; Pei, Z.; Feng, Q.; Zhu, Z. Preload Loss in Uncoated Weathering Steel Bolted Connections Considering Corrosion and Fatigue. *J. Constr. Steel Res.* **2024**, *221*, 108921. [CrossRef]
8. Hao, C.; Luo, J.; Wang, B.; Zhang, X.; Gan, L. Causes of Stiffness Degradation in Steel–UHPC Composite Beam-Bolted Connections. *Buildings* **2023**, *13*, 2064. [CrossRef]

9. *EN 1993-1-8*; Eurocode 3: Design of Steel Structures—Part 1–8: Design of Joints. European Committee for Standardisation: Brussels, Belgium, 2005.
10. Maggi, Y.I.; Gonçalves, R.M.; Leon, R.T.; Ribeiro, L.F.L. Parametric Analysis of Steel Bolted End Plate Connections Using Finite Element Modeling. *J. Constr. Steel Res.* **2005**, *61*, 689–708. [CrossRef]
11. Liu, X.; Hao, Z.; Luo, X.; Jin, Z. Experimental Behavior and *Modelling* of Steel Bolted T-Stub Connections. *Buildings* **2023**, *13*, 575. [CrossRef]
12. Bursi, O.S.; Jaspart, J.P. Benchmarks for Finite Element Modelling of Bolted Steel Connections. *J. Construct. Steel Res.* **1997**, *43*, 17–42. [CrossRef]
13. Neves, L.A.C.; Cruz, P.J.S.; Henriques, A.A.R. Reliability Analysis of Steel Connection Components Based on FEM. *Eng. Fail. Anal.* **2001**, *8*, 29–48. [CrossRef]
14. Al-Khatab, Z.; Bouchaïr, A. Analysis of a Bolted T-Stub Strengthened by Backing-Plates with Regard to Eurocode 3. *J. Constr. Steel Res.* **2007**, *63*, 1603–1615. [CrossRef]
15. Francavilla, A.B.; Latour, M.; Piluso, V.; Rizzano, G. Simplified Finite Element Analysis of Bolted T-Stub Connection Components. *Eng. Struct.* **2015**, *100*, 656–664. [CrossRef]
16. Qiang, X.; Shu, Y.; Jiang, X.; Xiao, Y. Nonlinear Analysis on Mechanical Behaviour of High Strength Steel Extended Endplate Connections and Equivalent T-Stubs in Fire Considering Axial Force. *Case Stud. Constr. Mater.* **2023**, *19*, e02402. [CrossRef]
17. Qiang, X.; Zhang, Z.; Jiang, X.; Wang, M. Study on Initial Stiffness of High Strength Steel T-Stubs Considering Bending Stiffness of Bolts. *J. Build. Eng.* **2023**, *76*, 107273. [CrossRef]
18. Yapici, O. Advanced Finite Element Modelling of Stainless Steel Bolted T-Stubs under Large Deformations. *Structures* **2023**, *58*, 105461. [CrossRef]
19. Wang, Y.; Sun, L.; Wang, P.; Hou, G.; Cai, X.; He, M. Feasibility Study of TSOB Replacing Standard High-Strength Bolt in T-Stub Connection. *Structures* **2024**, *62*, 106246. [CrossRef]
20. Jin, X.; Liu, L.; Yu, S.; Wang, P.; Liu, M.; Yan, Y.; Huang, X. Tensile Behavior of TOBs Bolted T-Stub to Circular Steel Tube with Reverse-Channel. *J. Constr. Steel Res.* **2024**, *217*, 108626. [CrossRef]
21. Kameshki, E.S. Discrete Optimum Design of Steel Frames by Genetic Algorithm. *J. King Saud Univ. Eng. Sci.* **2003**, *15*, 217–233. [CrossRef]
22. Dede, T.; Bekirolu, S.; Ayvaz, Y. Weight Minimization of Trusses with Genetic Algorithm. *Appl. Soft Comput.* **2011**, *11*, 2565–2575. [CrossRef]
23. Ho-Huu, V.; Nguyen-Thoi, T.; Vo-Duy, T.; Nguyen-Trang, T. An Adaptive Elitist Differential Evolution for Optimization of Truss Structures with Discrete Design Variables. *Comput. Struct.* **2016**, *165*, 59–75. [CrossRef]
24. Tang, H.; Lee, J. Chaotic Enhanced Teaching-Based Differential Evolution Algorithm Applied to Discrete Truss Optimization. *Structures* **2023**, *49*, 730–747. [CrossRef]
25. Cucuzza, R.; Aloisio, A.; Rad, M.M.; Domaneschi, M. Constructability-Based Design Approach for Steel Structures: From Truss Beams to Real-World Inspired Industrial Buildings. *Autom. Constr.* **2024**, *166*, 105630. [CrossRef]
26. Habashneh, M.; Movahedi Rad, M. Plastic-Limit Probabilistic Structural Topology Optimization of Steel Beams. *Appl. Math. Model.* **2024**, *128*, 347–369. [CrossRef]
27. Habashneh, M.; Cucuzza, R.; Domaneschi, M.; Movahedi Rad, M. Advanced Elasto-Plastic Topology Optimization of Steel Beams under Elevated Temperatures. *Adv. Eng. Softw.* **2024**, *190*, 103596. [CrossRef]
28. Grubits, P.; Cucuzza, R.; Habashneh, M.; Domaneschi, M.; Aela, P.; Movahedi Rad, M. Structural Topology Optimization for Plastic-Limit Behavior of I-Beams, Considering Various Beam-Column Connections. *Mech. Based Des. Struct. Mach.* **2024**, 1–25. [CrossRef]
29. Ribeiro, T.; Bernardo, L.; Carrazedo, R.; De Domenico, D. Eurocode-Compliant Topology Optimisation and Analysis of a Steel Cover-Plate in a Splice Moment Connection. *Mater. Today Proc.* **2022**, *65*, 1056–1063. [CrossRef]
30. Wang, H.; Yang, H.; Qian, H.; Chen, D.; Jin, X.; Fan, F. Static Experimental Analysis and Optimization of Innovative Pre-Engineered Tubular Section Beam-Column Connections in Cold-Form Steel Frames. *J. Build. Eng.* **2022**, *48*, 103989. [CrossRef]
31. Bathe, K.-J. *Finite Element Procedures*, 2nd ed.; Pearson: London, UK, 2014; Volume 2, ISBN 9780979004957.
32. Kramer, O. *Genetic Algorithm Essentials*; Springer International Publishing: Cham, Switzerland, 2017.
33. Balogh, T.; Vigh, L.G. Optimal Fire Design of Steel Tapered Portal Frames. *Period. Polytech. Civ. Eng.* **2017**, *61*, 824–842. [CrossRef]
34. Di Trapani, F.; Sberna, A.P.; Marano, G.C. A New Genetic Algorithm-Based Framework for Optimized Design of Steel-Jacketing Retrofitting in Shear-Critical and Ductility-Critical RC Frame Structures. *Eng. Struct.* **2021**, *243*, 112684. [CrossRef]
35. Li, G.; Li, Z.; Zeng, Q.; Guo, X. Shape Optimization of Cast Steel Tubular Joints Based on Subdivision Surface and Genetic Algorithm. *Thin-Walled Struct.* **2024**, *204*, 112258. [CrossRef]
36. Cucuzza, R.; Rad, M.M.; Domaneschi, M.; Marano, G.C. Sustainable and Cost-Effective Optimal Design of Steel Structures by Minimizing Cutting Trim Losses. *Autom. Constr.* **2024**, *167*, 105724. [CrossRef]

37. Okwu, M.O.; Tartibu, L.K. *Metaheuristic Optimization: Nature-Inspired Algorithms Swarm and Computational Intelligence, Theory and Applications*; Springer: Cham, Switzerland, 2021.
38. Syswerda, G. Simulated Crossover in Genetic Algorithms. *Found. Genet. Algorithms* **1993**, *2*, 239–255.
39. Gonçalves, J.F.; Resende, M.G.C. A Parallel Multi-Population Genetic Algorithm for a Constrained Two-Dimensional Orthogonal Packing Problem. *J. Comb. Optim.* **2011**, *22*, 180–201. [CrossRef]
40. Yang, J.; Soh, C.K. Structural Optimization by Genetic Algorithms with Tournament Selection. *J. Comput. Civ. Eng.* **1997**, *11*, 195–200. [CrossRef]
41. Goldberg, D.E.; Deb, K. A Comparative Analysis of Selection Schemes Used in Genetic Algorithms. *Found. Genet. Algorithms* **1991**, *1*, 69–93.
42. Michael, S. *ABAQUS/Standard User's Manual, Version 6.9*; Dassault Systèmes Simulia Corp.: Johnston, RI, USA, 2009.
43. *AXISVM Version X7 User's Manual*; Inter-Cad Mérnöki Szoftver Kft.: Budapest, Hungary, 2024.
44. Der, B.; Wald, F.; Vild, M. Numerical Design Calculation of T-Stubs at Elevated Temperatures. *Fire Technol.* **2024**, 1–22. [CrossRef]
45. Bezerra, L.M.; Bonilla, J.; Silva, W.A.; Matias, W.T. Experimental and Numerical Studies of Bolted T-Stub Steel Connection with Different Flange Thicknesses Connected to a Rigid Base. *Eng. Struct.* **2020**, *218*, 110770. [CrossRef]
46. *EN 1993-1-5*; Eurocode 3: Design of Steel Structures—Part 1–5: General Rules—Plated Structural Elements. European Committee for Standardisation: Brussels, Belgium, 2006.
47. Ivanyi, M.; Baniotopoulos, C.C. *Semi-Rigid Connections in Structural Steelwork*; Springer: Wien, Austria, 2000.
48. Gödrich, L.; Wald, F.; Kabeláč, J.; Kuříková, M. Design Finite Element Model of a Bolted T-Stub Connection Component. *J. Constr. Steel Res.* **2019**, *157*, 198–206. [CrossRef]
49. Miller, B.L.; Goldberg, D.E. Genetic Algorithms, Tournament Selection, and the Effects of Noise. *Complex. Syst.* **1995**, *9*, 193–212.
50. Martins, J.P.; Correia, J.; Ljubinković, F.; Simões da Silva, L. Cost Optimisation of Steel I-Girder Cross-Sections Using Genetic Algorithms. *Structures* **2023**, *55*, 379–388. [CrossRef]
51. Hassanat, A.; Almohammadi, K.; Alkafaween, E.; Abunawas, E.; Hammouri, A.; Prasath, V.B.S. Choosing Mutation and Crossover Ratios for Genetic Algorithms-a Review with a New Dynamic Approach. *Information* **2019**, *10*, 390. [CrossRef]